Journal of Nuclear Materials 378 (2008) 333–340

Contents lists available at ScienceDirect

Journal of Nuclear Materials

journal homepage: www.elsevier.com/locate/jnucmat

Investigation of passive films on nickel Alloy 690 in lead-containing environments

B. Peng [a], B.T. Lu [a], J.L. Luo [a,*], Y.C. Lu [b], H.Y. Ma [c]

[a] Department of Chemical and Materials Engineering, University of Alberta Edmonton, Alberta, Canada T6G 2G6
[b] Component Life Technology, Station 80, Atomic Energy of Canada Ltd., Chalk River Laboratories, Chalk River, Ontario, Canada K0J 1J0
[c] Department of Chemistry, Shandong University, Jinan, Shandong 250100, PR China

ARTICLE INFO

Article history:
Received 8 December 2007
Accepted 23 June 2008

PACS:
62.20.Mk
28.52.Fa
82.45.Bb

ABSTRACT

Passive films formed on Alloy UNS N06690 were investigated in simulated crevice chemistries. It was found the role of lead in corrosion processes is strongly dependent on the pH value of the testing solutions. At pH 1.5 the effect of lead is narrowly noticeable; while at pH 12.7, lead has a significant influence on the electrochemical performance of alloy UNS N06690. The lead alters the surface morphologies at both pH and account for higher hydroxide content in the surface film at pH 12.7. The lead incorporation hinders the formation of spinel oxides during the passivation in alkaline solution. Nanoindentation tests indicate a significant lead-induced degradation in the mechanical properties of passive films. The passivation degradation is attributed to detrimental effects of lead via interrupting the dehydration process and hindering the formation of protective layers on the alloy surface.

1. Introduction

Stress corrosion cracking (SCC) of steam generator (SG) tubing materials is of great concern with reference to the safety of nuclear power generation systems. It has been reported that the presence of lead contamination in the feedwater on the secondary side can increase the SCC susceptibility of the SG tubing materials, especially nickel-based alloys [1,2]. In order to improve lead-induced SCC (PbSCC) resistance, nickel Alloy 690 has been developed to replace Alloy 600 as SG tubing materials by means of optimizing the alloy composition. The content of chromium in Alloy 690 was substantially increased, which was proved to be beneficial to its SCC resistance. However, PbSCC in this type of nickel alloy still reportedly occur, especially in caustic environments [1,3,4]. This is to some extent contradictive to the common knowledge that stainless steels and nickel alloys are the best choices in alkaline aggressive conditions. Several PbSCC mechanisms, such as liquid metal embrittlement [1], selective grain boundary oxidation [2] and hydrogen embrittlement [5], have been proposed, but none of them gives a completely interpretation to the PbSCC phenomena. In recent decades, experimental evidences revealed that the susceptibility of PbSCC is related to the instability of passive films [1,6,7]. With the formation of passive films, the crack growth rate is essentially determined by anodic dissolution rate of materials and film rupture rate [8]. From this point of view, corrosion resistance and mechanical properties of the passive film play a key role in the initiation and propagation of SCC. However, literature review shows that few studies were carried out to investigate the characteristics and properties of passive films on nickel alloys. Only basic concepts are far from enough to clarify the role of lead in the passivity of nickel alloys. It is important, therefore, to scrutinize the passivation process of nickel alloys in the presence of lead and provide a better understanding of the effect of lead on passivity on SG tubing materials.

In present work, corrosion resistance of Alloy 690 was evaluated at different pH values. The morphology, composition, structure and mechanical response of passive films formed in various chemistries were examined by SEM, XPS, SIMS, XRD analyses and nanoindentation. The characteristics of Pb-doped passive films have been presented.

2. Experimental procedures

2.1. Test solution

A set of special solutions were designed to simulate CANDU[1] SG crevice chemistries, as shown in Table 1. To investigate the effect of lead on the electrochemical performance of the nickel alloy samples, 0.22 mM PbO was added as lead contaminations to basic solutions. PbO was selected because it is the most common lead compound found in the crack in tubing materials.

* Corresponding author. Tel.: +1 780 492 2232; fax: +1 780 492 2881.
E-mail address: jingli.luo@ualberta.ca (J.L. Luo).

[1] CANDU is the trade mark of Atomic Energy of Canada, Ltd.

0022-3115/$ - see front matter © 2008 Elsevier B.V. All rights reserved.
doi:10.1016/j.jnucmat.2008.06.037

Table 1
Compositions of testing solutions (mM)

No.	NaCl	KCl	Na_2SO_4	$CaCl_2$	$NaHSO_4$	NaOH	PbO	pH 25 °C
1	300	50	150	150	0	400	0	12.7
2	300	50	150	150	0	400	2.2	12.7
3	300	50	150	150	50	0	0	1.5
4	300	50	150	150	50	0	2.2	1.5

2.2. Test material and sample preparation

The testing material is nickel-based tubing material UNS N06690. The nominal composition in weight percent is 0.02C, 30Cr, 10Fe, 0.5Mn, 0.5Si and Ni in balance. The samples for electrochemical measurement were mounted with epoxy and mechanically grounded up to 600 grit SiC paper. Then the surface was rinsed with de-ionized water, degreased in acetone and dried with compressed air before use.

For surface analysis, alloy UNS N06690 was cut into 1×2 cm^2 pieces. The specimens were grounded with silicon paper up to 600-grit, cleaned in de-ionized water and degreased with acetone. Then the specimens were divided into 4 groups according to the 4 groups of testing chemistries (see Table 1). Each group of specimens was put into an autoclave and immersed in the corresponding solutions for 24 h at 300 °C. The solutions in the autoclave were deaerated continuously with pure nitrogen gas one hour prior to the heating till the end of the sample preparation. During this process, surface films were formed on the sample surfaces. After taken out of the autoclave all the specimens were cleaned in acetone by ultrasonic machine and were ready for XPS and SIMS analysis.

2.3. Electrochemical measurements

A conventional three-electrode cell was used in the experiments. A saturated calomel electrode (SCE) was used as the reference electrode and a long and coiled platinum wire as the counter electrode. All experiments are carried out at room temperature (23 °C). Prior to electrochemical measurements, the solution was deaerated with pure nitrogen gas for 1 h which was continued through all experiments. Before each electrochemical test, the sample was preconditioned at $-1.0\ V_{SCE}$ for 900 s to remove the air formed film. Metallic lead was electrodeposited on the sample surface during this period. The dynamic potential scanning began from −0.2 V less than the open circuit potential (OCP) to the designated positive potential, with a scanning rate of 1 mV/s.

2.4. XPS analysis

All samples were prepared by immersing in designated simulated SG crevice solutions at 300 °C for 24 h. The XPS measurements were performed using an Axis-ULTRA (Kratos Analytical) spectrometer controlled by a SUN workstation. Photoelectron emission was excited by an aluminium (monochromatized) source operated at 210 W with initial photon energy 1486.71 eV. The survey spectra were recorded at steps of 0.33 eV using 160 eV pass energy, whereas high resolution spectra were taken at steps of 0.1 eV using 20 eV pass energy. The base pressure was approximately 5×10^{-10} Torr. The C1s peak from adventitious carbon at 284.6 eV was used as a reference to correct the charging shifts. The photoelectrons were collected at a take-off angle of 90° with respect to the sample surface. Depth profiling was performed over an area of 1.5×1.5 mm^2 under 3 keV Ar-ion sputtering and the sputter rate was estimated to be 3 nm/min. The high resolution spectra were fitted according to the Gaussian–Lorentzian lineshape, and the Shirley approach was used to subtract backgrounds. The O1s core level curve fitting theoretically shows three components at 530 ~ 531 eV, 531 ~ 532 eV and 532 ~ 533 eV, [9] which corresponds to the binding energy of oxygen in M–O–M, M–OH and H_2O-M bonds, respectively. Cr 2p3/2 core level generally can be decomposed into three contributions, a hydroxide one, an oxide one and a metallic one with binding energies located at 577.4 ± 0.5 eV, 576.0 ± 0.5 eV, 574.0 ± 0.1 eV [9–11]. Before XPS analysis, the morphologies of the same samples were examined with JEOL Field Emission SEM.

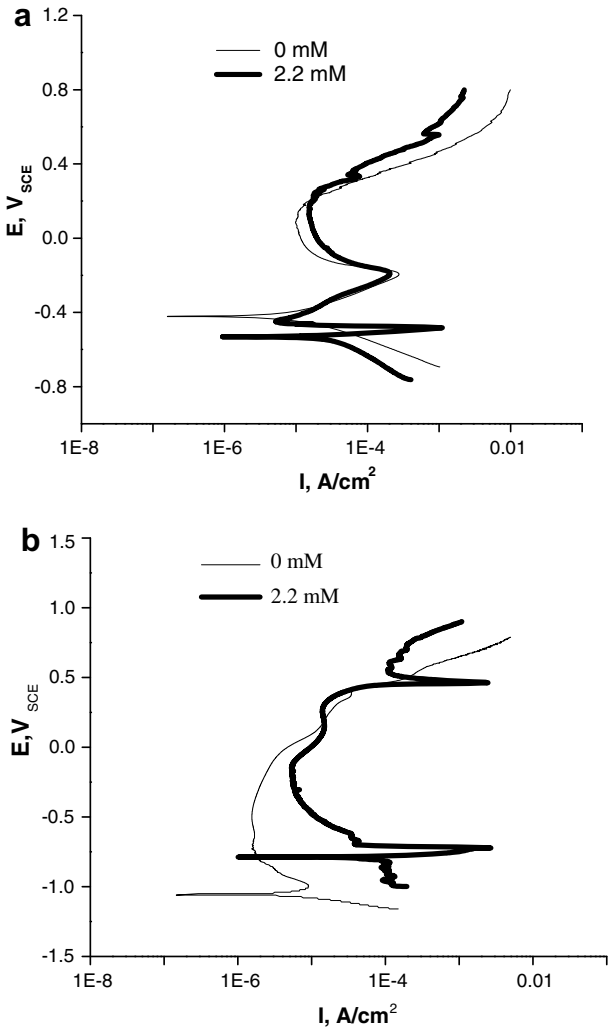

Fig. 1. Polarization plots of UNS N06690 alloy in: (a) acid and (b) alkaline solutions with and without lead. Scan rate: 1 mV/s.

2.5. SIMS analysis

The same samples in XPS analysis were used for Time-of-Flight Secondary Ion Mass Spectroscopy (ToF SIMS) tests. SIMS analysis was carried out with ToF SIMS IV instrument (ION-TOF Gmbh). In the current work, the analysis source used was Ga^+, operation at 15 kV; the sputtering source is Cs^+, operating at 1 kV.

2.6. X-ray diffraction analysis

The X-ray diffraction experiment was carried out by using Rigaku rotating anode RU-200B system equipped with a Cobalt anode as X-ray source. A690 samples passivated in different SG crevice chemistries for 24 h at 300 °C were cut and thinned to an approximate thickness of 1 mm. The sample surfaces were cleaned with acetone in ultrasonic cleaning machine prior to the XRD experi-

ment. Thin film setup (vs. wide angle) was used in this study. The incident angle θ was 0.5°.

2.7. Nanoindentation test

The nanoindentation apparatus (Hysitron Co., Ltd., Triboscope®) was attached with AFM (Digital Instruments, Nanoscope E) to control the positioning and displacement of the indenter on the specimen surface. A diamond cube corner indenter was used in the experiment. Prior to any indentation experiment, the instrument was calibrated with the standard fused silicon sample. A triangular load function was employed for the indentation consisting of a 5-s loading segment and a 5-s unloading segment.

The measurement of reduced modulus and hardness is sensitive to the surface condition of samples. For Alloy 690 samples passivated at high temperature, the surface is not uniform and smooth. Considering that these factors may affect the experimental result, nanoindentation was conducted at comparatively smooth sites, and average values were calculated after the experiments.

3. Results

3.1. Polarization behavior

Fig. 1 shows the effect of lead on the polarization behaviors of Alloy 690 at different pH values. In acidic solutions (pH 1.5), the polarization curves obtained in the solutions with and without lead are very similar, including nearly identical active–passive transition potential and trans-passivation potential, and similar current densities in the active region, as can be seen in Fig. 1(a). Even so, one can still find the influence of lead on the polarization behavior of Alloy 690. For example, a current peak related to the oxidation of lead appears at $-0.48\ V_{SCE}$ in the lead-containing solution, and passive current slightly increases in the passive region (from -0.2 to $0.2\ V_{SCE}$) as compared with that in absence of lead. In contrast, the decrease of corrosion resistance caused by lead impurities seems more obvious in the case of alkaline solution (pH 12.7). The oxidation of lead takes place at more negative potential ($-0.78\ V_{SCE}$). The passive current is enhanced to a considerable degree by the presence of lead, especially at low potential region (from $-0.78\ V_{SCE}$ to $0\ V_{SCE}$). More interestingly, a secondary current peak is observed at $0.45\ V_{SCE}$, which may be attributed to the valence change of lead in the surface film.

3.2. Surface morphology

The surface morphologies of Alloy 690 samples are similar to a degree in both lead-free (Fig. 2(a)) and lead-containing (Fig. 2(b)) acidic solutions except a relatively rough surface in the latter case, when the samples are passivated in the acidic solutions. However, for the sample prepared in the alkaline solution without lead, a crystalline surface layer completely covers the sample surface, as indicated in Fig. 3(a); whereas in the presence of lead, a needle-like surface layer covers the surface, as shown in Fig. 3(b). Comparing Fig. 2 with Fig. 3, it is concluded that the influence of lead

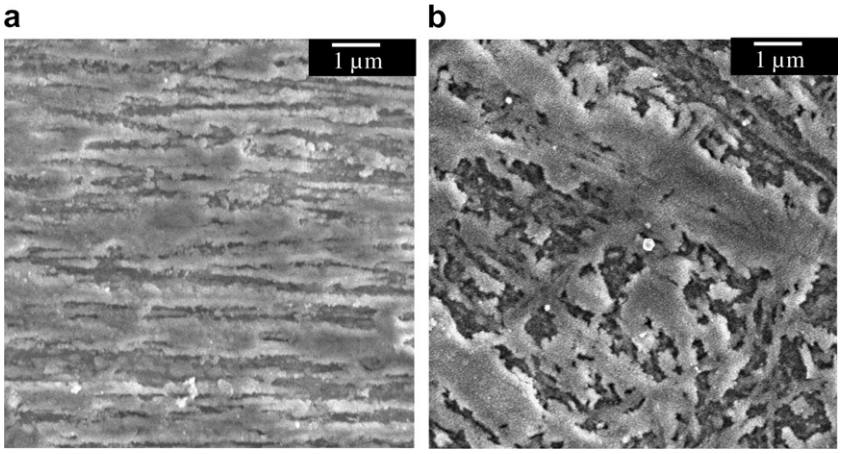

Fig. 2. SEM images of Alloy 690 immersed in acid solution for 24 h at 300 °C: (a) without PbO and (b) with 2.2 mM PbO.

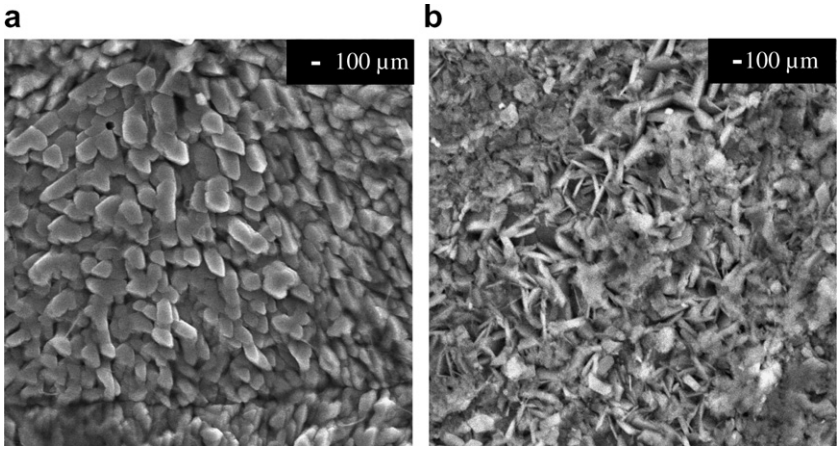

Fig. 3. SEM images of UNS N06690 alloy immersed in CANDU alkaline solution for 24 h at 300 °C: (a) without and (b) with 2.2 mM PbO.

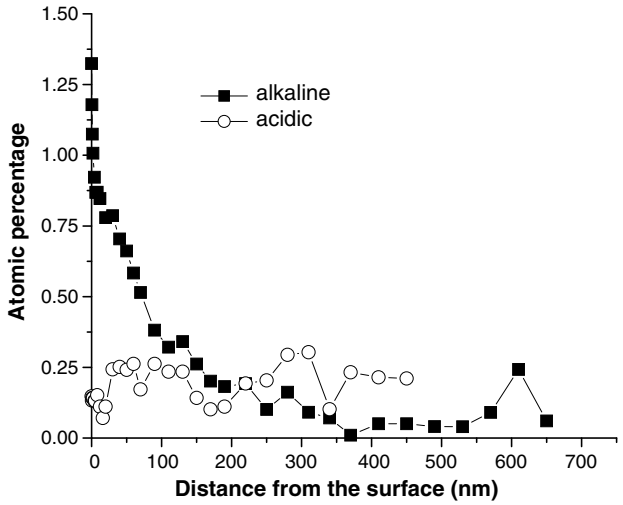

Fig. 4. Depth profiles of Pb in the passive films on UNS N06690 alloy passivated at 300 °C in Pb-containing SG crevice chemistries.

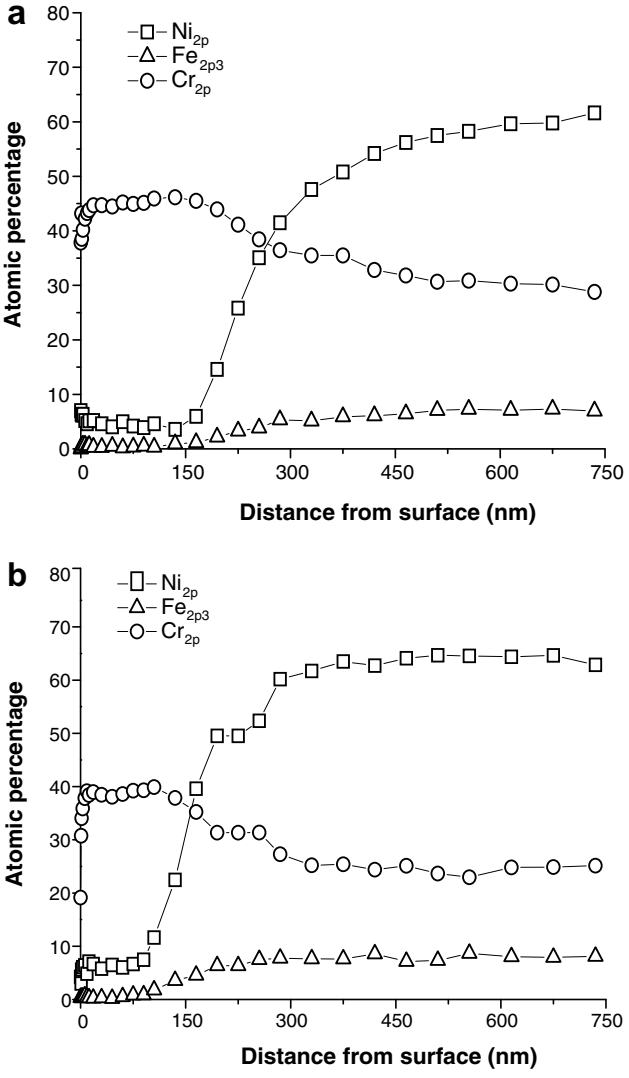

Fig. 5. Composition profiles for passive films on UNS N06690 alloy prepared at 300 °C in acidic SG crevice solutions: (a) without and (b) with 2.2 mM PbO.

impurities on the surface morphology is more significant when the material is exposed in alkaline SG crevice environment.

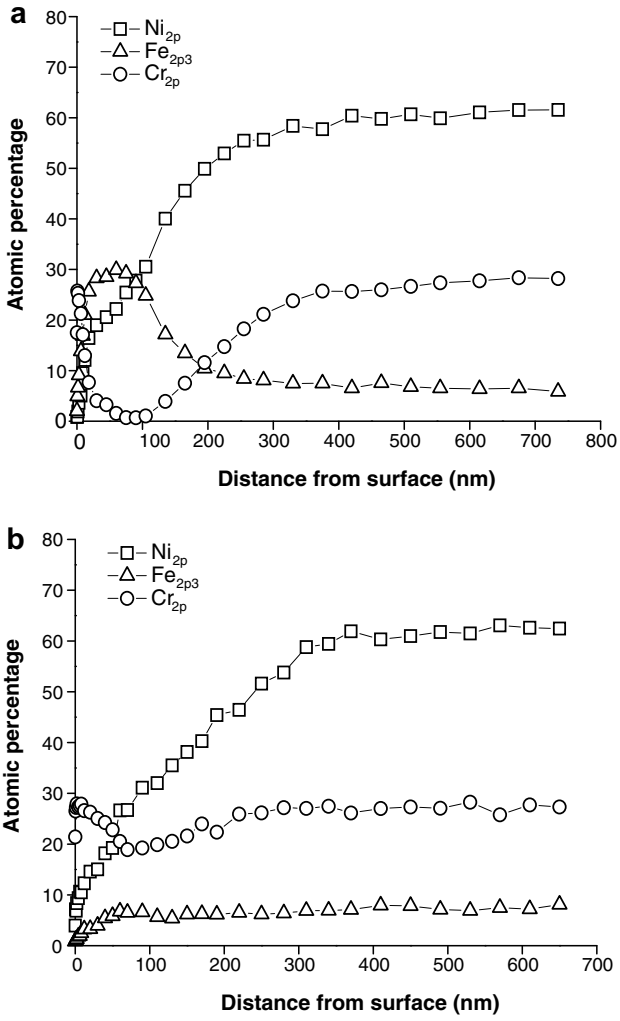

Fig. 6. Composition profiles for passive films on UNS N06690 alloy prepared at 300 °C in alkaline SG crevice solutions: (a) without and (b) with 2.2 mM PbO.

3.3. Changes in composition and structure of passive films

Fig. 4 shows the depth profile of lead in the passive films of Alloy 690 with respect to different pH conditions. It is evident that lead was involved in the formation of passive films and the content and distribution of lead varies in different pH environments. On the other hand, the protective property of passive films fundamentally depends on their compositions and structures. Fig. 5 depicts depth-composition profiles of passive films formed in acidic SG crevice solutions. We have not found much difference for each element regardless of the presence of lead. On the contrary, in the case of alkaline solutions, the presence of lead caused a significant change of chromium profile, as shown by Fig. 6. In the film without lead, a Cr depleted layer can be detected just beneath the outmost layer. However, the chromium content greatly increased with the incorporation of lead.

According to Okamoto et al. [12,13], there are generally three types of bonds in passive films, i.e. O-M, OH-M, and H_2O-M. The distribution of oxide and hydroxide in the passive film can be identified by deconvolution of O_{1s} high resolution spectra. Fig. 7 shows that the presence of lead contamination in alkaline solutions leads to a significant increase in the amount of hydroxyl in the passive film (Fig. 7(b)); while it hardly affects the ratio of OH^-/O^{2-} in the passive films formed in acidic solutions (Fig. 7(a)).

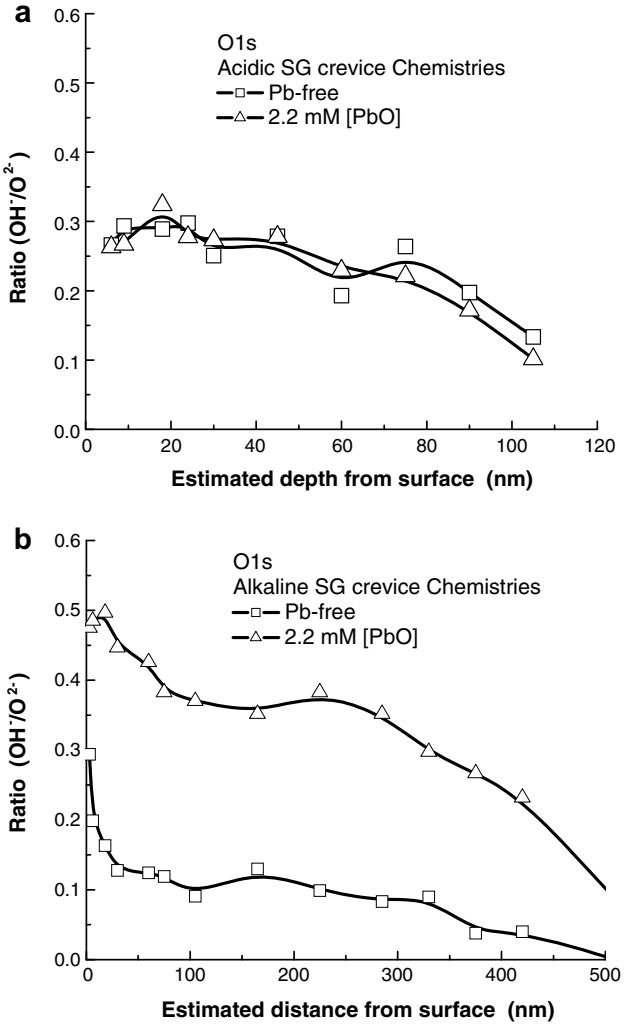

Fig. 7. The distributions of the ratio of OH^- to O^{2-} in the passive films obtained in: (a) acidic and (b) alkaline solutions at 300 °C with and without 2.2 mM PbO.

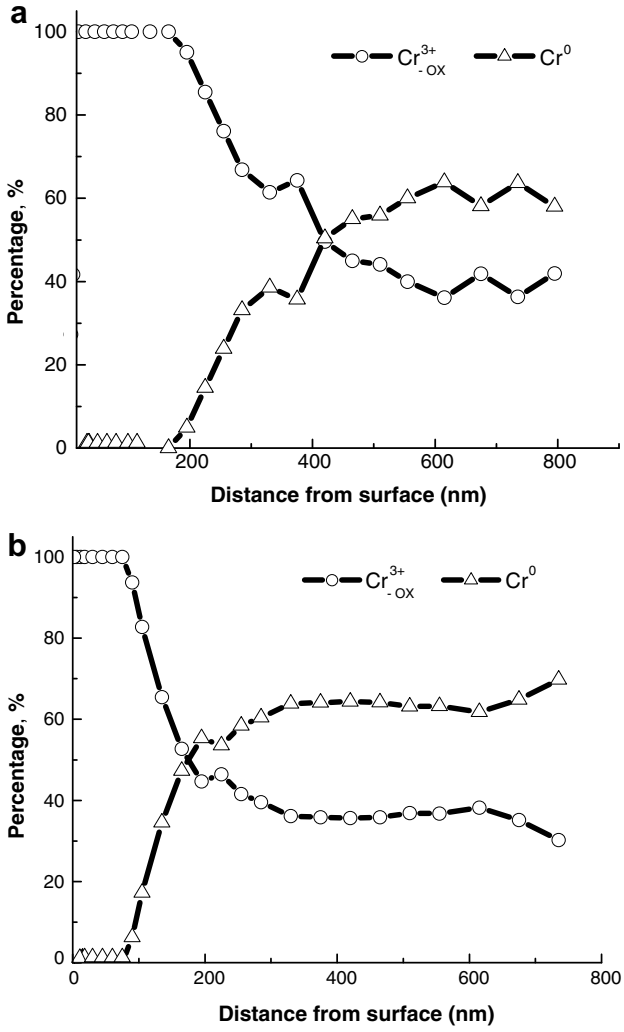

Fig. 8. XPS $Cr_{2p3/2}$ spectra for UNS N06690 alloy passivated in acidic solutions at 300 °C: (a) without and (b) with 2.2 mM PbO.

The $Cr_{2p3/2}$ core level spectra also reflect the trend of OH^-/O^{2-} distribution in the films. In the films obtained in acidic solutions, no hydroxide can be detected regardless of the presence of lead, as shown in Fig. 8. This agrees with that fact that the role of lead is not pronounced in the acidic solution. However, a large amount of hydroxide appears in the film obtained in alkaline solutions, as illustrated in Fig. 9, indicating that the hydroxide concentration is substantially increased with the presence of lead.

SIMS profiles of hydroxide and hydrogen in sample surfaces for the samples prepared in alkaline solutions have been further investigated since XPS technique cannot identify the distribution of hydrogen in the surface film. In Fig. 10, the content of hydroxide is higher in the surface film formed in the solution with lead than that without lead, which is in good agreement with XPS results. At the same time, hydrogen contents in the samples have shown the same trend as the hydroxide, suggesting the ingress of lead also increases the total hydrogen concentration in the film.

3.4. Retarded formation of spinels

In order to evaluate the effect of hydroxide contents in the films on the structure of surface layers on the alloy, passive films prepared in different solutions were examined by means of low angle XRD. In the acidic solutions, as shown in Fig. 11, the ingress of lead has no obvious influence on the structure of passive films on Alloy 690. The peaks of γ phase reflect the signals excited from the substrate. No crystalline structure is detected in the passive film regardless of the presence of lead. In the case of alkaline condition, spinel structure clearly appears in the passive film passivated in the lead-free solution, as presented in Fig. 12(a), whereas lead impurities completely inhibit the formation of the bi-metal oxides in the same solution. It is known that spinel oxides are important barriers to improve the dissolution resistance for nickel alloys at high temperatures [14].

3.5. Mechanical properties of passive films

The changes of composition and structure in passive films can result in the deviation of their mechanical properties. Fig. 13 demonstrates that the hardness dropped for the passive films on Alloy 690 passivated in both acidic and alkaline solutions as a result of lead contamination. The values of the hardness decrease with increasing indentation depth, h_c, regardless of the presence of lead. This phenomenon is acknowledged as the indent size effect [15,16]. The results clearly indicate a deleterious effect of Pb on the mechanical properties of the surface film. Furthermore, it is obvious that the lead caused degradation of film hardness is more pronounced in high pH solution.

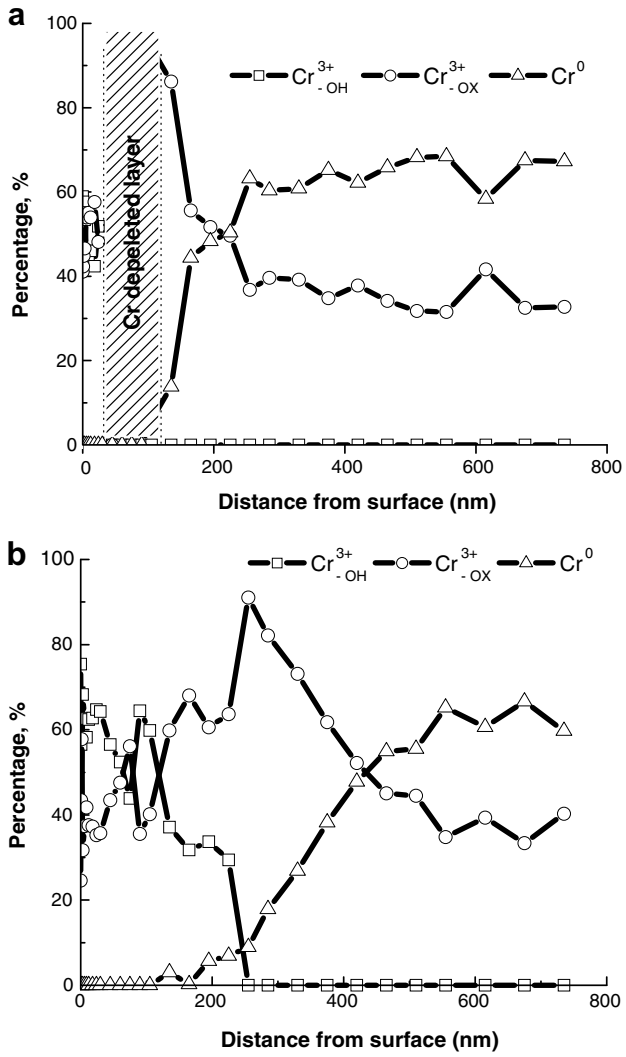

Fig. 9. XPS $Cr_{2p3/2}$ spectra for UNS N06690 alloy passivated in alkaline solutions at 300 °C: (a) without and (b) with 2.2 mM PbO.

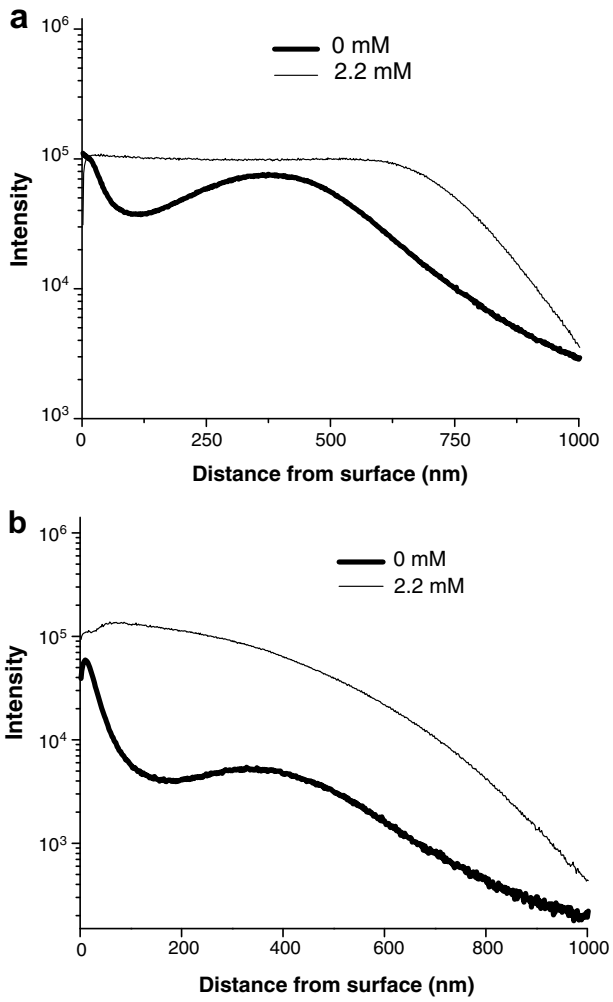

Fig. 10. Distribution profiles of: (a) hydroxide and (b) hydrogen for UNS N06690 alloy immersed in alkaline solutions with and without 2.2 mM PbO at 300 °C.

4. Discussion

Based on the experimental results, it should be noted that, in alkaline lead-containing solution the corrosion resistance of Alloy 690 decreases although the increase of chromium content in the passive film was observed. The classical theory of passivity indicates that the higher chromium content in alloys will result in rapid repassivation and lower corrosion susceptibility of materials. When bulk chromium content is more than 13% (wt%) in the alloy, a compact oxide film can be developed quickly in corrosive environments, providing excellent anti-corrosion performance. In the present work, it was found that the passive film obtained in alkaline solutions with lead comprises more chromium hydroxides, instead of chromium oxides. It is well acknowledged that the production of crystalline oxides in passive film is highly dependent on dehydration reaction during aging process [12,13]. Therefore, the inhabitation of crystallization by lead is naturally a result of retarded dehydration in passive film. Taking into account the increasing chromium and hydroxide contents in the passive film due to lead contamination in alkaline solution, it implicates that in a lead-containing environment the instability of the passive film on Alloy 690 results from the detrimental effect of lead, which fundamentally modifies the composition, structure and mechanical properties of the passive film. The efficient use of alloy chromium in the material is essentially interrupted by lead.

It has been pointed out that the effect of metal ions on the stability of passive films is closely related to their chemical hardness [17]. According to the Lewis rule of acids and bases, metal ions are acids and act as electron acceptors, while ligands are bases and behave as electron donors [18,19]. The reaction between acids and bases leads to the formation of metal complexes. Acids and bases can be further quantitatively characterized by hard and soft nature based on the hard and soft acid and base (HSAB) concept. The stability of the A:B combination is essentially depends on the bond between A and B. In HSAB theory it is assumed that a hard–hard bond or a soft-soft one will generate a higher stabilization. During corrosion process, the following reaction may take place at the initial stage

$$M^{2+} + H_2O = M(OH)^{+} + H^{+}, \quad (1)$$

$$M(OH)^{+} = MO + H^{+}. \quad (2)$$

It was reported that hard metal ions prefer to attract H_2O and OH^- in the passive film and are classified as hard bases or acids. In the Ni–Cr–Fe–Pb system, the hardness sequence is $Fe^{3+} > Cr^{3+} > Ni^{2+} > Fe^{2+} > Pb^{2+}$ [20]. Cr and other alloying metal ions are expected to combine with OH^- or H_2O quickly in a lead-free solution and enhance the repassivation of the alloy. With the presence of lead, the deproton reaction of $M^{2+} \cdot H_2O$ may be inhibited due to the low-

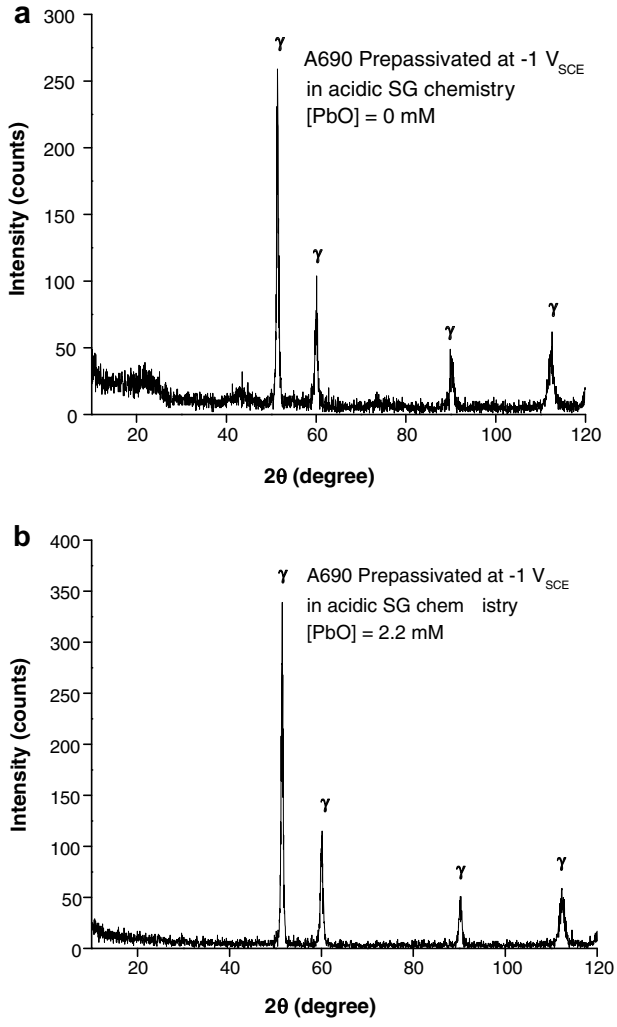

Fig. 11. XRD patterns of samples passivated in acidic solutions at 300 °C: (a) without and (b) with 2.2 mM PbO.

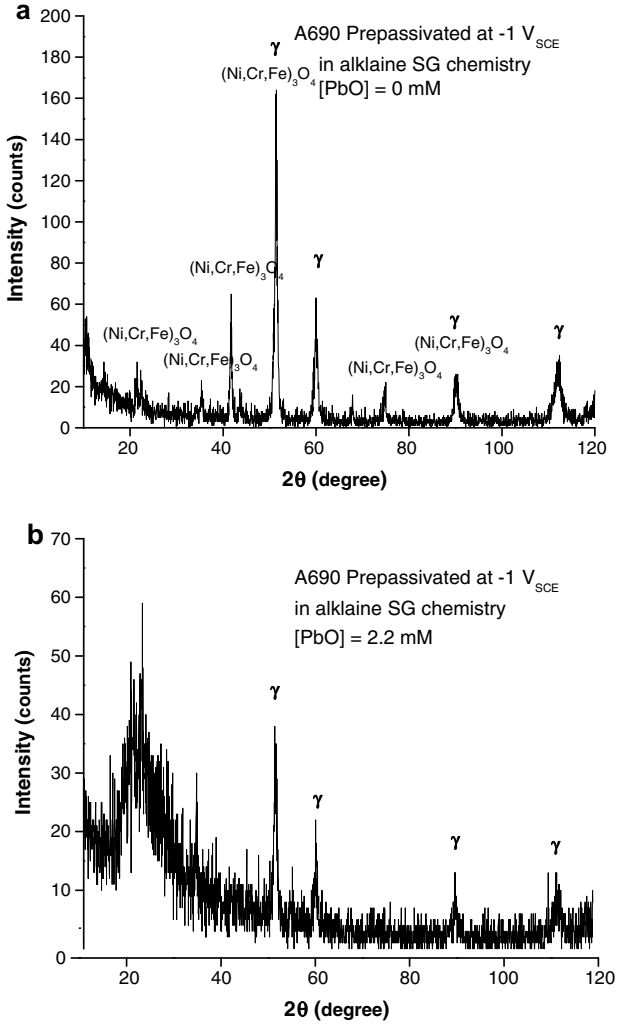

Fig. 12. XRD patterns of samples passivated in alkaline solutions at 300 °C: (a) without and (b) with 2.2 mM PbO.

er affinity of Pb and OH^-, resulting in a passive film with higher hydroxide and lower corrosion resistance.

In alkaline solutions, lead complex is stable and lead species can be adsorbed at the exposed fresh surface. Lead ions may migrate into the gel-like hydrated oxide layer and occupy cation vacancies. The dehydration of lead-containing hydroxides may gradually evolve into the development of a lead-doped surface film [21].

$$Pb(OH)_2 + 2Ni(OH)_2 \rightarrow (OH)Ni{-}O{-}Pb{-}O{-}Ni(OH) + H_2O, \quad (3)$$

$$Pb(OH)_2 + 2Cr(OH)_3 \rightarrow (OH)_2Cr{-}O{-}Pb{-}O{-}Cr(OH)_2 + H_2O, \quad (4)$$

$$Pb(OH)_2 + 2Fe(OH)_2 \rightarrow (OH)Fe{-}O{-}Pb{-}O{-}Fe(OH) + H_2O, \quad (5)$$

$$Pb(OH)_2 + 2Fe(OH)_3 \rightarrow (OH)_2Fe{-}O{-}Pb{-}O{-}Fe(OH)_2 + H_2O. \quad (6)$$

Further maturation leads to the formation of a 'lead-doped' oxide film, which may possess different electrochemical and mechanochemical properties. The detrimental effects of lead have been already demonstrated in our previous and present investigations [21].

$$(OH)Ni{-}O{-}Pb{-}O{-}Ni(OH) \rightarrow 2NiO \cdot PbO + H_2O, \quad (7)$$

$$(OH)_2Cr{-}O{-}Pb{-}O{-}Cr(OH)_2 \rightarrow Cr_2O_3 \cdot PbO + 2H_2O, \quad (8)$$

$$(OH)Fe{-}O{-}Pb{-}O{-}Fe(OH) \rightarrow 2FeO \cdot PbO + H_2O, \quad (9)$$

$$(OH)_2Fe{-}O{-}Pb{-}O{-}Fe(OH)_2 \rightarrow Fe_2O_3 \cdot PbO + 2H_2O. \quad (10)$$

Considering our key observations, combined with other publications [8,22] it is reasonable to draw an analogy and construct a similar framework of a film rupture model based on the available experimental evidence. This model for SCC on Alloy 690 in lead-containing alkaline environments can be interpreted as follows [21].

- Assume the rupture of the passive film on Alloy 690 can take place under tensile stress.
- In alkaline solutions, a lead complex such as $HPbO_2^-$ is stable and lead species can be adsorbed at the exposed fresh surface.
- Lead ions will migrate into the gel-like hydrated oxide layer and occupy the cation vacancies.
- Lead is involved in the film formation process, resulting in the passivity degradation. The instability of the passive film is reflected by enhanced anodic dissolution and slow repassivation rate. As a consequence, an accelerated crack growth rate and creep rate can be expected.
- The Pb-doped passive film possesses more sensitive mechanical properties, which increases the probability of localized passive film breakdown.
- This process repeats and eventually leads to premature failure of tubing materials.

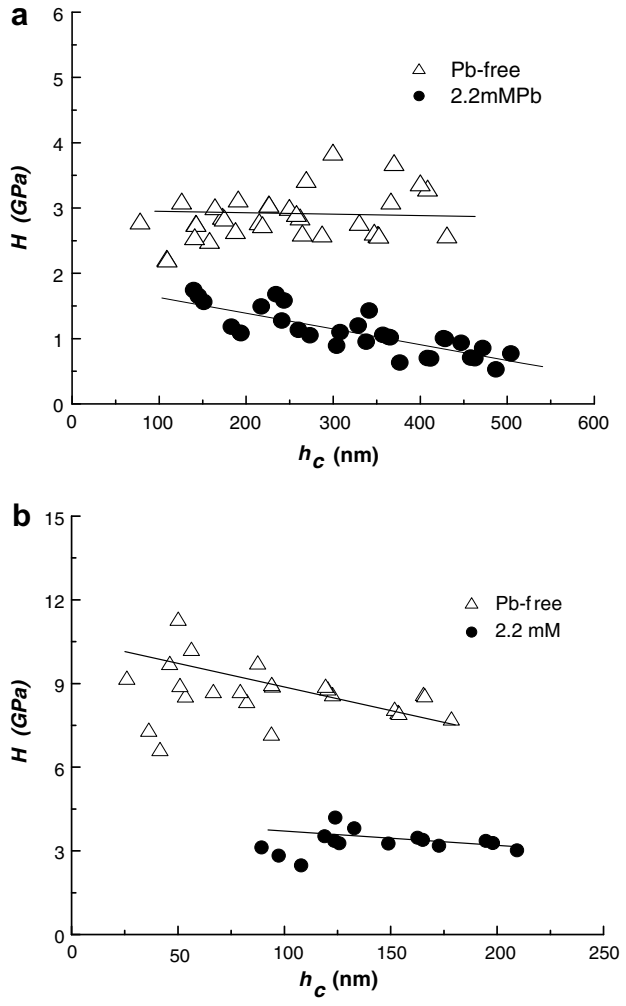

Fig. 13. Hardness of the passive film on Alloy 690 passivated in: (a) acidic and (b) alkaline crevice solutions with and without 2.2 mM PbO at 300 °C.

5. Conclusions

The deleterious effect of lead on the corrosion resistance of Alloy 690 is strongly dependent on pH value of the testing solution. The enhanced anodic dissolution and film modification by lead is more significant in alkaline environments than in acidic media.

Surface analysis reveals that in alkaline solutions, lead increases hydroxide concentration in the passive film. This change reduces beneficial effect of chromium in the alloy and decreases the resistance of film breakdown.

When passivated in acidic and alkaline solutions, the mechanical properties of passive films decrease with the presence of lead and the hardness difference is more pronounced in high pH condition.

Lead inhibits the formation of crystal structure in the passive film in alkaline condition; this may be attributed to the retarded dehydration during aging process. However, this deleterious effect is not very obvious in acidic condition.

Acknowledgements

This work was supported by NSERC/Atomic Energy of Canada Ltd (AECL) CRD Grant. R.L. Tapping, and P. Angell of AECL are acknowledged for supporting this work. The authors would like to appreciate J. Kaminski and M. Dupuis of AECL for carrying out the high temperature surface treatments, D. Karpuzov and A.Q. He in Alberta Centre for Surface Engineering and Science, University of Alberta, for their assistance in performing, SEM, XPS and SIMS measurements and Shiraz Merali for XRD measurements.

References

[1] R.W. Staehle, J.A. Gorman, Corrosion 59 (2003) 931;
R.W. Staehle, J.A. Gorman, Corrosion 60 (5–63) (2004) 115.
[2] J. Lumsden, A. Mcllree, R. Eaker, Mater. Sci. Forum 475–479 (2005) 1387.
[3] D.L. Harrod, R.E. Gold, R.J. Jacko, Light Water Reactors (2001) 14.
[4] M.L. Castano-Marin, D. Gomez-Briceno, F. Hernandez-Arroyo, in: Proceedings of the 6th International Symposium on Environmental Degradation of Materials in Nuclear Power System, 1993.
[5] M.J. Psaila-Dombrowski, F.H. Hua, in: Proceedings of the 9th International Symposium on Environmental Degradation of Materials in Nuclear Power System, 1999, p. 703.
[6] T. Sakai, N. Nakagomi, T. Kikuchi, Corrosion 54 (1998) 515.
[7] R. Kilian, IAEA Specialist Meeting on Steam Generator Problems and Replacement, International Atomic Energy Agency, Madrid Spain, 1993, p. 137.
[8] F.P. Ford, P.L. Andresen, Corros. Mech. (1994) 501.
[9] J.F. Moulder, W.F. Stickle, P.E. Scobol, K.D. Bomben, Handbook of X-ray Photoelectron Spectroscopy, Perkin Elmer, Eden Prairie, MN, 1992.
[10] R.S. Dutta, A. Lobo, R. Purandare, et al., Metall. Mater. Trans. A 33A (2002) 1437.
[11] M.J. Carmezim, A.M. Simoes, M.F. Momntemor, M. Da Cunha Belo, Corros. Sci. 47 (2005) 581.
[12] G. Okamoto, T. Shibata, R. Frankenthal, J. Kruger, Electrochemical Society, Springer, 1978, p. 646.
[13] G. Okamoto, Corros. Sci. 13 (1973) 471.
[14] L.L. Shreir, R.A. Jarman, G.T. Burstein, Corrosion, third ed., vol. 2, Springer, 1994.
[15] N.A. Flick, J.W. Hutchinson, J. Mech. Phys. Solid 41 (1993) 825.
[16] N.A. Flick, G.A. Muller, M.F. Ashby, et al., Acta Metall. Mater. 42 (1994) 475.
[17] S.H. Zhang, T. Shibata, T. Haruna, Corros. Sci. 47 (2005) 1049.
[18] G.N. Lewis, Valence and Structure of Atoms and Molecules, Chem. Catalogue Co. Inc., New York, 1923.
[19] G.N. Lewis, J. Franklin Inst. 226 (1938) 293.
[20] M. Misono, E. Ochiai, Y. Saito, Y. Yoneda, J. Inorg. Nucl. Chem. 29 (1967) 2685.
[21] B.T. Lu, J.L. Luo, Y.C. Lu, J. Electrochem. Soc 154 (2007) C379.
[22] S.J. Ahn, V.S. Rao, H.S. Kwon, U.C. Kim, Corros. Sci. 48 (2006) 1137.